Ultrafast-laser-radiation transfer in heterogeneous tissues with the discrete-ordinates method

Zhixiong Guo and Kyunghan Kim

Here light propagation and radiation transfer of ultrafast laser pulses in heterogeneous biological tissues are simulated by use of the discrete-ordinates method (DOM). Formulations for solving the time-dependent radiation-transfer equation are deduced for three-dimensional geometries incorporating the Fresnel specularly reflecting boundary condition and characteristics of ultrafast laser pulses. The present method can treat both the incident laser intensity and the scattered radiation intensity from the walls of the targeted tissue as two components, i.e., a diffuse part and a specular part. Reflectivity at the tissue–air interface is calculated by use of Snell's law and the Fresnel equation. The high-order S_{10} DOM method is found to be adequate for describing the propagation and transfer of ultrafast laser radiation in heterogeneous tissues. The time-dependent radiation field in the tissue as well as the temporal radiation intensity profiles at the boundaries can be obtained simultaneously. The absolute values of the logarithmic slope of the temporal reflectance and transmittance at various detector positions are found to converge to a constant value in a homogeneous tissue model. With the inclusion of a small inhomogeneity, such a value will change in line with the property of the embedded inhomogeneity. The orientation of heterogeneity of the tissues also substantially affects the radiation intensity at the boundaries. The effect of the Fresnel boundary in the modeling is pronounced. The simulated transmitted signals are broadened and amplified under specularly reflecting boundary condition as compared with those under diffusely reflecting boundary conditions.

OCIS codes: 170.5280, 170.6920, 030.5620, 140.7090, 000.4430.

1. Introduction

Recent research has suggested that light scattering and absorption can provide a valuable, noninvasive means of quantitatively probing tissue morphology.[1–6] Light radiation absorption has been broadly applied to applications in biomedical treatment such as laser surgery[7,8] and photodynamic therapy[9–10] (PDT). The laser is also the excitation source in fluorescence imaging, scanning, and labeling.[11,12] Fundamental to these laser applications is laser radiation propagation and transfer in biological tissues, which is described by the radiation-transfer theory.

Modeling of light transport has traditionally been performed with either the Monte Carlo (MC) method[13–15] or deterministic methods based on the diffusion approximation (DA).[16] Generally the statistical MC method is time consuming, and its results are subject to statistical errors. The diffusion theory presumes that the scattering predominate and that the medium be optically diffuse so that the angle-dependent radiant intensity is replaced by an angle-independent photon flux and the Boltzmann radiative-transport equation is simplified as a diffusion equation. However, the diffuse approximation is hardly applicable to heterogeneous biological tissues with nonscattering or low-scattering regions;[6] moreover, experiments[17] have shown that it fails to match experimental data when the tissue sample is not optically diffuse. The development of accurate simulation of radiation transport in heterogeneous media is in demand.

The discrete-ordinates method (DOM) has become one of the most popular methods for solving Boltzmann transport equations for radiation transfer and neutron transport. This is because (1) the DOM can be accomplished to high-order accuracy, (2) the derivation of DOM schemes is relatively simple, and (3) the DOM is compatible with the finite-difference or finite-element schemes for specular or diffuse phenomena. Studies on almost every aspect of the

The authors are with the Department of Mechanical and Aerospace Engineering, Rutgers, The State University of New Jersey, Piscataway, New Jersey 08854. Z. Guo's e-mail address is guo@jove.rutgers.edu.

Received 7 August 2002; revised manuscript received 16 November 2002.

0003-6935/03/162897-09$15.00/0

DOM applicable to multidimensional radiative heat transfer have been reported.[18–21] However, most of the previous DOM algorithms focused on the solution of steady-state radiation-transfer equations (RTEs) because the effect of time-dependent light propagation is negligible in traditional heat-transfer problems.

With the advent of the ultrafast laser and its broad applications in biomedical technologies, the study of time-dependent laser radiation transfer incorporating radiation propagation with the speed of light has become increasingly important. Recently the time-dependent DOM method has been explored to one-dimensional[22,23] and multidimensional geometries.[24,25] Yet the media were not characterized tissues. Fresnel's reflection was not taken into account, nor was the ultrafast laser pulse considered in these studies. Klose *et al.*[6] used a DOM algorithm as a forward model for optical tomography. But the DOM there is time independent (steady state) and has only 24 discrete ordinates (equivalent to the S_4 quadrature scheme) in the spatial angle direction. The DOM S_4 method is easily subjected to the ray effect and false scattering as pointed out by Chai *et al.*[26] because of the limited number of discrete ordinates. Instead, high-order quadratures such as S_8 (80 discrete ordinates) and S_{10} (120 discrete ordinates) are more commonly adopted in the radiation heat-transfer community. Nevertheless, to our knowledge these high-order schemes have not been applied to the study of ultrafast-laser-radiation transfer in heterogeneous tissues.

In the present study the time-dependent DOM is formulated for ultrafast-laser-radiation transfer in anisotropically scattering, absorbing, and emitting tissues in three-dimensional (3D) rectangular enclosures. The S_{10} quadrature scheme is adopted in most calculations. Both the temporal radiation intensity on the boundaries and the radiation field inside the tissue are computed. The novelty of the present method involves the incorporation of the transient effect, the Fresnel effect, and the heterogeneous effect. In this study we aim at the development and demonstration of an accurate radiation-transfer modeling for ultrafast laser applications in biomedical systems that span a broad range from the forward model in optical tomography, fluorescence excitation and imaging, laser welding and surgery, to PDT, and so on. Different application requires different information. For example, the prediction of temporal radiation intensity along the boundaries is needed in optical tomography, whereas the knowledge of radiation energy deposition and/or irradiance is paramount in fluorescence excitation, laser tissue welding, and PDT. The emphasis of most studies in photon migration has been placed on the identification of boundary radiation intensity. Few studies have addressed time-dependent radiation deposition and/or irradiance, which are extremely influential for fluorescence imaging, microscopy and spectroscopy.

With the incorporation of the transient effect, i.e., radiation propagation with the speed of light, the present study focuses mainly on applications of laser propagation and energy transfer for times of the order of those required for radiation to travel along with a path length through the geometry being considered. A typical time order can be calculated with a simple formula, $t = L/c$, in which L is the characteristic length and c is the speed of light in the medium. For example, the considered tissue depth is usually in the range from several millimeters to dozens of millimeters; the time scale is then of the order of dozens of picoseconds (the refractive index is $\sim$1.40 for tissue). Even with the consideration of pulse broadening in strongly scattering tissue, the time is of the order of 1 ns. Within such a time scale, heat-diffusion and heat-capacity effects are generally negligible such that the medium can be generally treated as "cold".

An important concern of this study is the Fresnel boundary effect that is induced at the tissue–air interface owing to the difference of refractive indices between air and biological tissue. The reflectivity and transmissivity at the interface are described by the Fresnel equation. With the use of Snell's law and the Fresnel equation, the specular reflectivity at each discrete angle direction can be calculated. For the sake of comparison, however, the reflection at the interface is assumed to be either specular or diffuse. If the reflection is assumed to be diffuse, diffuse reflectivity at the interface is an average of the predicted specular reflectivity at all directions. This diffuse approximation is examined as compared with the Fresnel specular boundary condition.

Another important concern is the heterogeneity of tissues. A good model must be capable of handling heterogeneity without increasing difficulty and complexity. This is an important trait of the present method. To study the influence of heterogeneity, two tissue models will be considered. The first one is a two-dimensional (2D) multilayered tissue phantom. The influences of tissue heterogeneity and the Fresnel boundary will be quantitatively examined after a benchmark comparison between the present DOM S_{10} method and several other numerical techniques. The second model is a 3D rectangular tissue phantom with a small inhomogeneous zone embedded in the center. The characteristics of the temporal radiation field and the temporal distribution of reflectance and transmittance will be discussed. The influence of inhomogeneity absorption property on the logarithmic slope of temporal signals will be scrutinized.

2. Mathematical Models

A. Governing Equations

Consider a collimated laser-pulse incidence upon a 3D rectangular biological tissue as shown in Fig. 1. The laser radiation transfer can be described by the

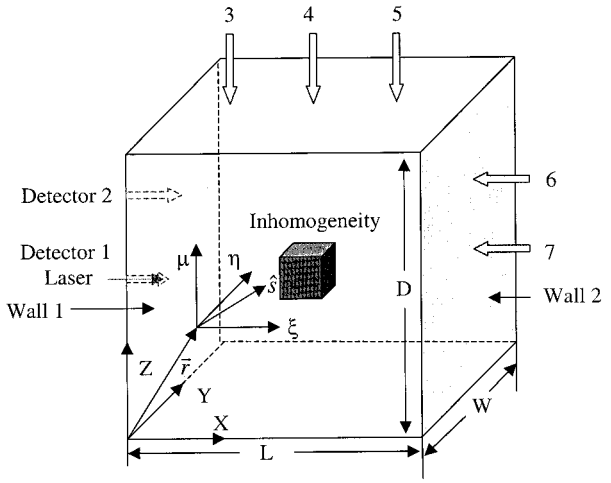

Fig. 1. Three-dimensional geometry and coordinates system.

time-dependent RTE formulated in each discrete-ordinate direction $\hat{s}^l$ as

$$\frac{1}{c}\frac{\partial I^l}{\partial t} + \xi^l \frac{\partial I^l}{\partial x} + \eta^l \frac{\partial I^l}{\partial y} + \mu^l \frac{\partial I^l}{\partial z} + \sigma_e I^l = \sigma_e S^l, \quad l = 1, 2, \ldots, n, \tag{1}$$

where ξ^l, η^l, and μ^l are the three direction cosines, I^l is the radiation intensity, σ_e is the extinction coefficient that is the sum of absorption coefficient, σ_a and scattering coefficient σ_s, c is the speed of light in the medium, and t is the time. S^l is the radiative source term and can be expressed as

$$S^l = (1-\omega)I_b + \frac{\omega}{4\pi}\sum_{i=1}^{n} w^i \Phi^{il} I^i + S_c{}^l, \quad l = 1, 2, \ldots, n, \tag{2}$$

in which the scattering albedo is $\omega = \sigma_s/\sigma_e$, Φ^{il} is the scattering phase function $\Phi(\hat{s}^i \rightarrow \hat{s}^l)$, I_b is the blackbody emitting intensity of the tissue, and $S_c{}^l$ is the source contribution of the collimated laser irradiation. The original integral term in Eq. (2) is represented by a sum of in-scattering radiation intensities in all discrete-ordinate directions. A quadrature set of n discrete ordinates with the appropriate angular weight w^l ($l = 1,2, \ldots, n$) is used. The choice of quadrature scheme is arbitrary, and studies on quadrature selection have been made by a number of researchers.[19–21]

The laser source $S_c{}^l$ in Eq. (2) is the driving force of the scattered laser propagation and transport in tissues. It is the in-scattering contribution of the collimated laser intensity in the discrete-ordinate direction $\hat{s}^l$,

$$S_c{}^l = \frac{\omega}{4\pi} I_c \Phi(\xi^c\xi^l + \eta^c\eta^l + \mu^c\mu^l), \tag{3}$$

where (ξ^c, η^c, μ^c) represents the collimated laser-incident direction. The normally incident laser intensity is distributed inside the tissue as

$$I_c(x, y, z, \xi_c, t) = I_0[x = 0, y, z, t - x/(c\xi_c)] \times \exp(-\sigma_e x/\xi_c)\delta(\xi_c - 1), \tag{4}$$

in which δ is the Dirac delta function and I_0 is the laser-beam intensity irradiated at the surface of the tissue. In general, the incident laser beam is of Gaussian profile in both time and spatial domains. Duhamel's superposition theorem[25] can be used to incorporate the effect of pulse width and shape of the ultrafast laser beam. It should be mentioned that Duhamel's theorem could be applied only to a linear system. The transient RTE is linear when only the radiation intensity is concerned as in the cases studied in the present paper. Since most transient radiative-transfer problems deal with ultrashort time scale and address the propagation of laser radiation, the medium emission is usually negligible, or the temperature of the medium is treated as "unchanged" during a short time.

B. Boundary Conditions

The boundaries are the tissue–air interfaces and assumed to be cold such that there is no radiation emission from the boundaries. We treat the interface as a plane surface. It can reflect and refract incident radiation. The refraction and reflection obey Snell's law and the Fresnel equation, respectively. Because the refractive index of tissue is greater than that of air, total reflection occurs when the incident angle θ_i of an internal radiation is not less than the critical angle $\theta_{cr} = \sin^{-1}(n_{air}/n_T)$. When $\theta_i < \theta_{cr}$, the reflectivity is calculated by Fresnel's equation as

$$\rho = \frac{1}{2}\left[\frac{\tan^2(\theta_i - \theta_r)}{\tan^2(\theta_i + \theta_r)} + \frac{\sin^2(\theta_i - \theta_r)}{\sin^2(\theta_i + \theta_r)}\right], \tag{5}$$

where θ_r is the refraction angle predicted by Snell's law.

In the Fresnel boundary condition, the reflection must be specular. However, the actual reflection at the interface may consist of both diffuse and specular components because the actual interface is not a smooth plane but one with a certain degree of roughness. The present method can treat both specular and diffuse components. For example, the diffuse intensity at wall with $x = 0$ is

$$I_w{}^d = \varepsilon_w I_{bw} + \frac{\rho_w{}^d}{\pi}\sum_{\xi^l<0}^{n/2} w^l I^l |\xi^l|, \tag{6}$$

and the specular intensity is

$$I_w{}^l = \rho_w{}^{sl} I^{-1}. \tag{7}$$

Here $\rho_w{}^d$ is the diffuse reflectivity of the interface and $\rho_w{}^{sl}$ is the specular reflectivity at direction $\hat{s}^l$. For comparison, the reflection is assumed to be either purely specular or purely diffuse in the present calculations. The diffuse reflectivity is a hemispherical average of specular reflectivity.

C. Numerical Schemes

The finite-volume approach[18] is employed to solve the transient RTE in its discrete-ordinate format. The positive scheme[20] is used to relate the upstream and downstream intensities in a control volume cell. The numerical schemes were introduced in a recent publication of Guo and Kumar.[25] Hence the details are not repeated here. However, it is worth pointing out that several new features have been added in the present study. These include Fresnel reflection, calculation of reflectivity, and treatment of characteristics of ultrafast laser pulses. In addition, the current subject of study is heterogeneous tissues or tissue phantoms with specific optical depths that are much larger than those considered in Guo and Kumar.[25] Further, the previous study focused on the examination of numerical accuracy and sensitivity of the transient DOM algorithm with various quadrature schemes (from S_8, S_{10}, S_{12}, S_{14}, to S_{16}) and time steps.

The number of discrete ordinates is $n = N \times (N + 1)$ in an S_N scheme. In the present study, the S_{10} scheme is adopted and its quadrature sets and corresponding angular weights are taken from the code TWOTRAN.[21] Thus we have to solve 120 coupled discrete-ordinate RTEs. It took ~8 h in the calculation for a 3D inhomogeneous problem with grid size of $27 \times 27 \times 27$ when a Dell personal computer (PC) with 1 CPU of Pentium III 500-MHz Xeon was used. If we lessen the order of the S_N scheme, the CPU time will be certainly reduced. For example, it took only 1.3 h when a S_4 scheme was used. However, this will affect accuracy. There is a trade-off between accuracy and efficiency for different applications. For example, accuracy is of the highest priority in the study of laser treatment and fluorescence imaging, whereas both accuracy and efficiency are important in optical tomography. With the rapid advance of computational technologies such as parallel computation and high-performance computers (currently 2.8-GHz Pentium IV PCs are available), efficiency will not be a problem in the near future.

3. Results and Discussion

At first, the present method is evaluated by means of a benchmark comparison in the study of ultrafast laser transport through a 2D rectangular enclosure with four different layers as shown in configuration I in Fig. 2(a). Four types of brain-tissue phantom are employed in the study, i.e., skull, cerebrospinal fluid (CSF), gray matter, and white matter. The optical properties of the four various tissues are assumed as follows. For skull tissue, $\sigma_a = 0.005\ \text{mm}^{-1}$ and $\sigma_s = 1.6\ \text{mm}^{-1}$. For CSF tissue, $\sigma_a = 0.001\ \text{mm}^{-1}$ and $\sigma_s = 0.01\ \text{mm}^{-1}$. For gray matter, $\sigma_a = 0.015\ \text{mm}^{-1}$ and $\sigma_s = 0.60\ \text{mm}^{-1}$. For white matter, $\sigma_a = 0.01\ \text{mm}^{-1}$ and $\sigma_s = 1.2\ \text{mm}^{-1}$. These values were used by several investigators[27] in a brain model. The present tissue model may serve as a benchmark model for others. The refractive indices of the four layers are assumed to be constant at 1.4. To study the effect of layer orientation, configuration II is arranged by means of exchanging the positions of the CSF and gray-matter layers in configuration I. The thickness and lateral width of the configurations are 35 and 20.2 mm, respectively. Eight detectors along the boundary of each configuration are selected for outputting temporal signals.

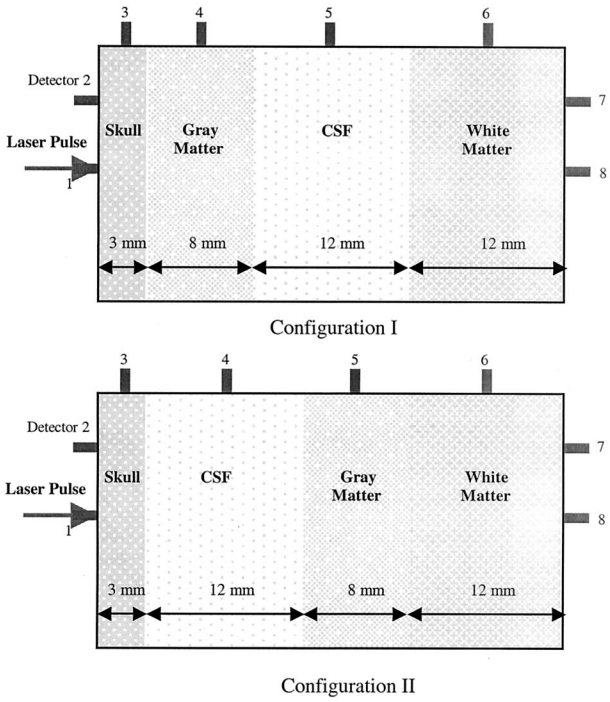

Fig. 2. Two-dimensional multilayered configurations: (a) configuration I, (b) configuration II.

Figure 3 shows comparisons of normalized transmittance at three selected detector positions between the DOM S_4 and S_{10} methods, DA, and MC method. It is seen that the S_{10} model gives the closest match with the MC predictions for all detector positions. The DA predictions differ from the MC ones in most time domains. The S_4 model also predicts relatively narrower transmitted distributions. The modeling of radiation transfer produces very smooth curves. However, the temporal profiles predicted by the MC method are slightly jagged in almost all detectors, although we have used a large number of photons (2×10^8) in the MC simulation. Further increasing the photon number will reduce the oscillation, but the improvement is very slow as compared with the rapid increase of photon number.

Then the influence of the Fresnel specularly reflecting boundary condition is examined in Fig. 4, where the temporal transmittance data are normalized by use of the corresponding peak values under diffusely reflecting boundary conditions. It is seen that the predicted magnitude of the transmittance under specularly reflecting conditions is greater than that under diffusely reflecting conditions. Also, the peak position for specular boundary shifts to a later time. At detector 5, which is located at the boundary of the CSF layer, the specular signal has an obvious

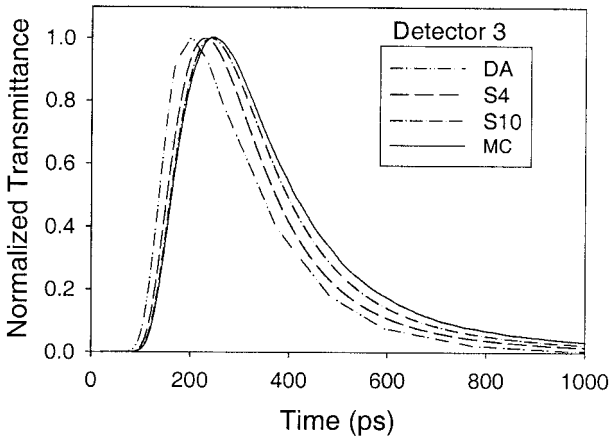

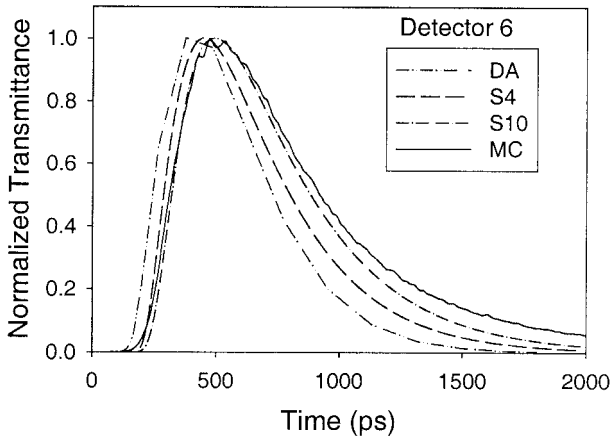

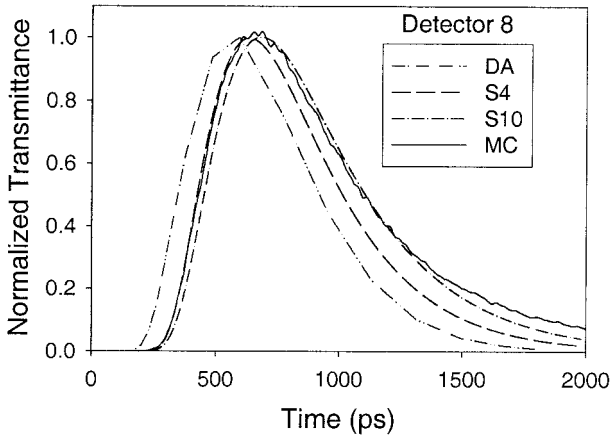

Fig. 3. Benchmark comparisons of temporal distributions of transmittances between DOM S_4 and S_{10} methods, DA, and MC method for ultrafast laser transport in 2D multilayered configuration I.

large broadening. In weakly scattering and absorption regions such as the CSF layer, light transport is decided mainly by its boundary condition. The results reveal that the radiation-transfer boundary is an important factor for the accurate prediction of photon transport in heterogeneous tissue. In all the calculations below, the Fresnel specularly reflecting boundary condition is used. In the popularly

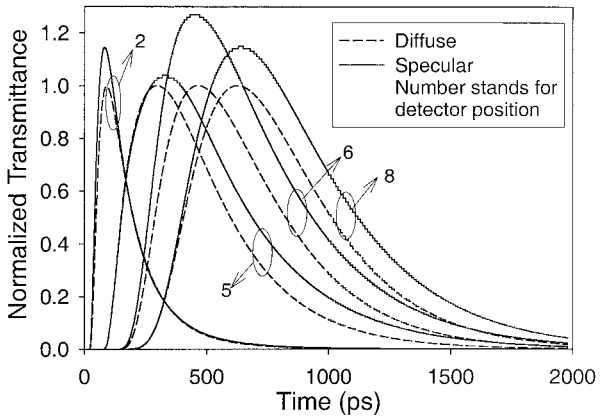

Fig. 4. Comparison of temporal transmittances between the Fresnel specular boundary and diffuse boundary conditions for configuration I.

adopted DA for photon migration in tissues, however, the Fresnel specular boundary condition cannot be incorporated.

Comparison of reflectance and transmittance between the two configurations is exhibited in Fig. 5, where results are normalized by the corresponding peak values for configuration II. At detector 1, the difference is invisible in this figure because the first skull layer in these two configurations is quite dense and the original impulsive laser pulse dominates the reflection. However, the difference in predictions between these two configurations is quite large for detectors from detector 2 to 7. Even though the overall optical properties along the pathway between the laser-incident spot and detector 8 are identical for these two configurations, there exists an appreciable difference of transmittance between these two cases at detector 8 because of the different orientation of CSF and gray-matter layers. This means that the orientation of the heterogeneous layers strongly affects the temporal signals. To determine the internal structure, the use of signals from just detectors 1 and 8 will not be sufficient.

Further inspecting the prediction differences at de-

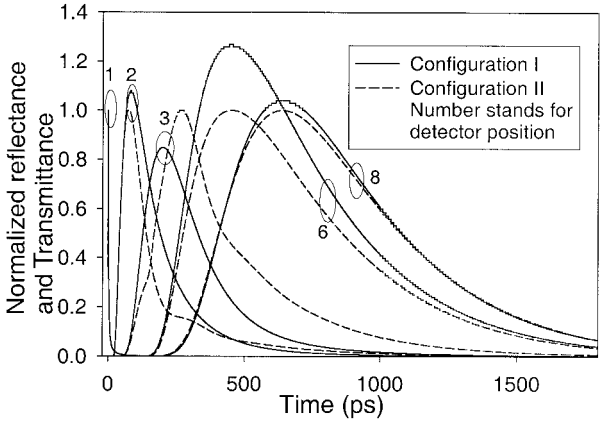

Fig. 5. Comparison of temporal reflectance and transmittance between configuration I and II.

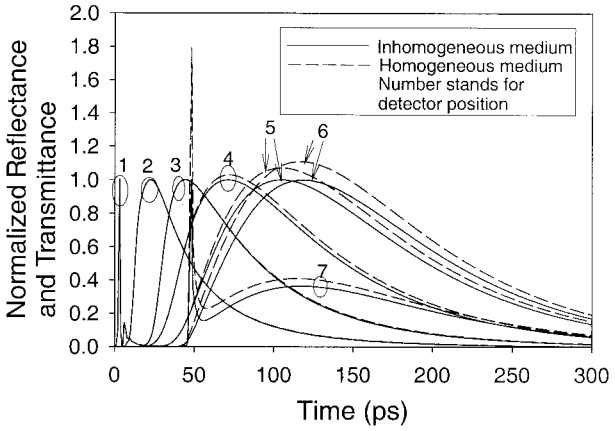

Fig. 6. Comparison of temporal reflectance and transmittance between homogeneous model and inhomogeneous model with a small inhomogeneity ($\sigma_a = 0.50\ \mathrm{mm}^{-1}$).

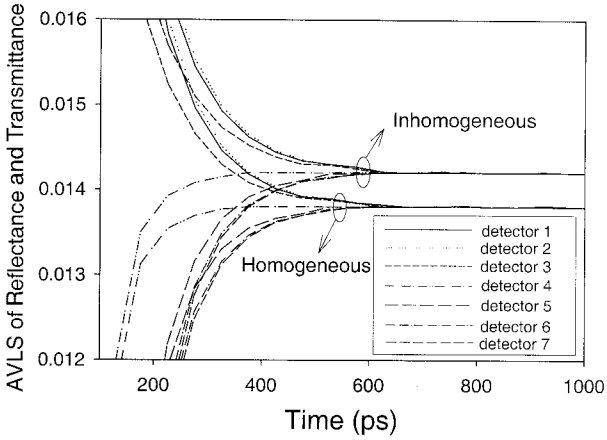

Fig. 8. Absolute value of log slopes of reflectance and transmittance at different detector positions for both homogeneous model and inhomogeneous model with a small inhomogeneity ($\sigma_a = 0.50\ \mathrm{mm}^{-1}$).

tector 8 and comparing these differences between Figs. 4 and 5, we find that the influence of tissue heterogeneity is even smaller than the effect of the modeling boundary condition, i.e., either specular surface or diffuse surface. A model incorporating inadequate interface conditions may lead to erroneous pictures. This strengthens our motivation in the present study to develop an accurate model by incorporating all realistic physical conditions.

The present method is finally applied to study the characteristics of ultrashort-laser-pulse transport through cubic tissue phantoms as shown in Fig. 1. The cubic side length is $L = W = D = 10$ mm. A small inhomogeneous zone with a side length of 1.2 mm is embedded at the center of the cube. In the inhomogeneous zone, the absorption coefficient varies from $\sigma_a = 0.01$, 0.02, 0.05, 0.10, 0.20, to 0.50 mm^{-1}, and the reduced-scattering coefficient[28] is kept at $\sigma_s' = 1.00\ \mathrm{mm}^{-1}$. In the surrounding tissue, $\sigma_a = 0.01\ \mathrm{mm}^{-1}$ and $\sigma_s' = 1.00\ \mathrm{mm}^{-1}$. The inhomogeneous zone with a larger absorption may be attributed to a malignant tumor, a concentrated photosensitizer, or an abnormality with an embedded fluorescent dye.

Figure 6 manifests the influence of inhomogeneity on the time-dependent reflectance and transmittance profiles. The temporal reflected or transmitted signals are normalized by use of the corresponding peak values in the case of the inhomogeneous model at all seven detector positions. In both the homogeneous ($\sigma_a = 0.01\ \mathrm{mm}^{-1}$ in the inhomogeneous zone) and heterogeneous ($\sigma_a = 0.50\ \mathrm{mm}^{-1}$ in the inhomogeneous zone) cases, the time with peak reflectance and/or transmittance and the broadening of the signal pulse width vary with the change of detector position. The distance between the laser-incident point and the detector, as well as the medium property between the source and detector, is an important factor for deciding the peak position and the pulse broadening. As the distance increases, the time of peak position, as well as the broadening of the pulse, enlarges. The difference in the temporal transmittance between the homogeneous medium and the heterogeneous one is obvious from detector 4 to 7. However, the difference from detector 1 to 3 is slight

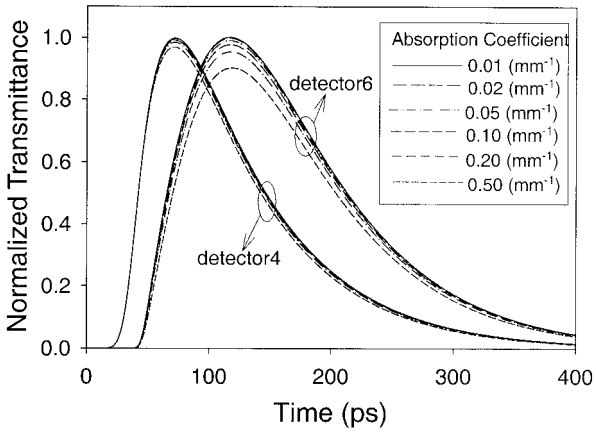

Fig. 7. Effect of absorption coefficient of the inhomogeneity on the temporal transmittance profiles.

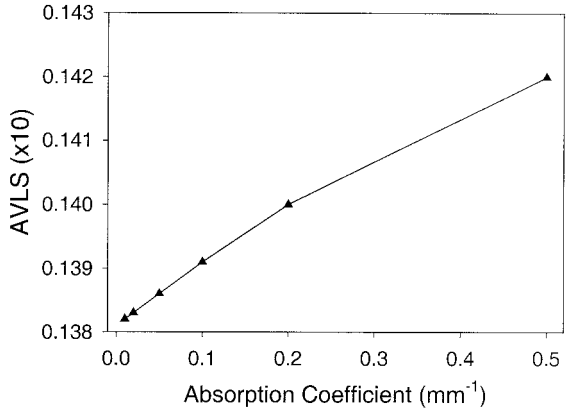

Fig. 9. Relationship between AVLS and absorption coefficient in the inhomogeneity.

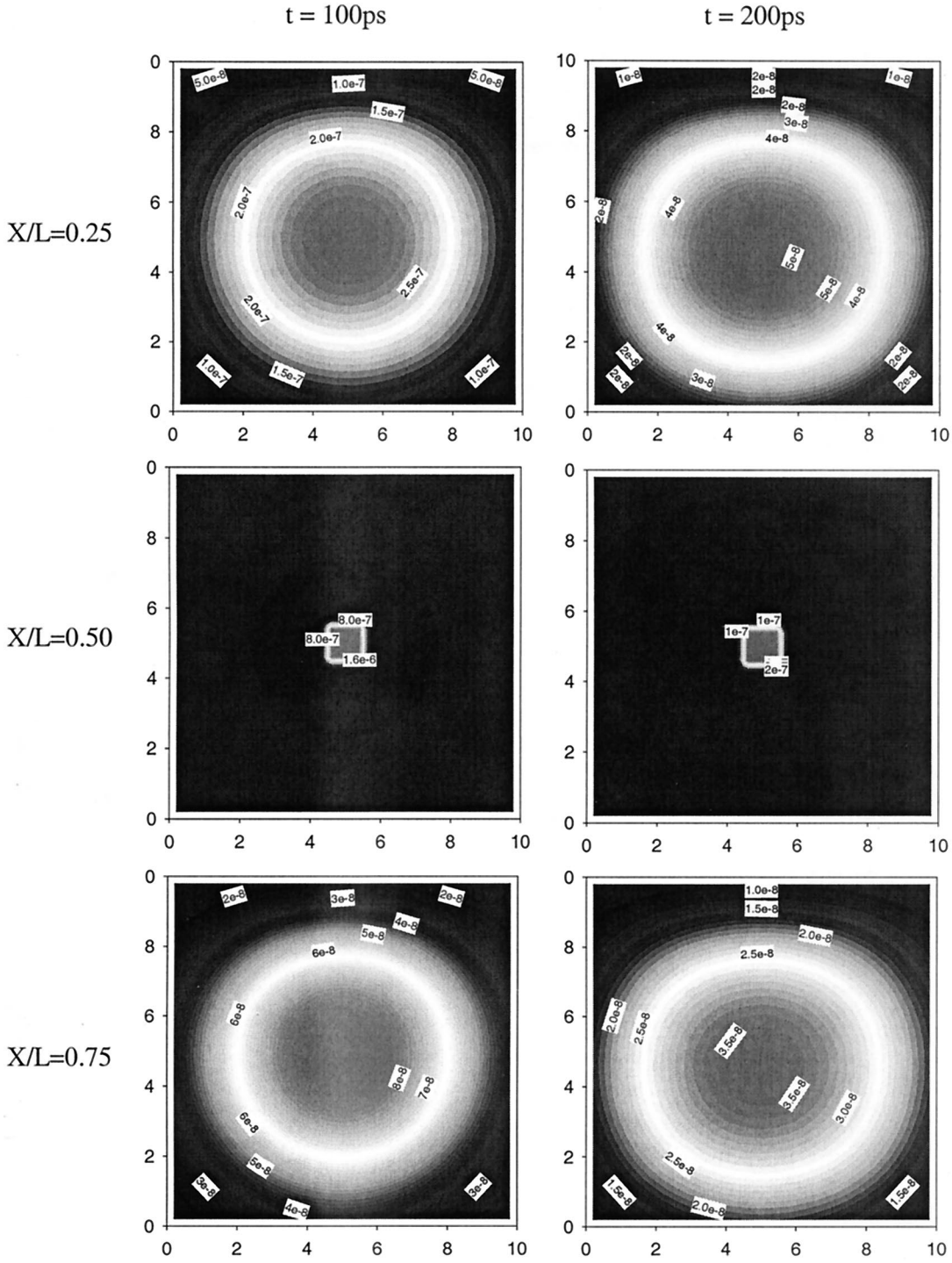

Fig. 10. Contour plots of divergence of radiative heat flux in Y–Z planes for inhomogeneous model with a small inhomogeneity ($\sigma_a = 0.10$ mm^{-1}) at the center.

in Fig. 6, but it will be visible if the signals are plotted in a logarithmic scale.

The absorption coefficient of the inhomogeneity may vary widely. The effect of varying absorption coefficient on the temporal transmittance profiles is demonstrated in Fig. 7. With the increase of absorption, the amplitude of the signals at the selected detectors is reduced and the difference in the signals between the normal homogeneous and inhomogeneous cases enlarges. Even with a minor increase of absorption (e.g., $\sigma_a = 0.02$ mm^{-1}), the difference is still visible. A quantitative analysis may help identify how to effectively enhance image contrast by injection of absorbing materials into targets.

Figure 8 shows the absolute values of logarithmic

slope (AVLS) of the temporal reflectance and transmittance for homogeneous and inhomogeneous models. The values of the AVLS converge to different constant values for homogeneous and inhomogeneous cases, respectively. Such a difference in the AVLS between the two different tissue models is detectable at all seven detector positions. The converged AVLS is purely a function of the medium property and is insensitive to the input laser pulse strength.

The AVLS versus absorption coefficient in the inhomogeneity is plotted in Fig. 9. It is found that the AVLS is almost linearly proportional to the absorption coefficient of the embedded inhomogeneity. This AVLS may be a perfect indicator for detecting the inhomogeneous absorbing zone. To our knowledge, such a finding has not been reported in the literature for heterogeneous tissues with a finite thickness and a small inhomogeneity. It may be explored for early detection of small tumors. Further detailed theoretical and experimental investigation will follow in the near future.[29]

The present method can be used to obtain the time-dependent radiation field that is routine in fluorescence imaging, laser treatment, and PDT. Figure 10 shows six contour plots of divergence of radiative heat flux (equivalent to energy deposition rate) at Y–Z planes at three selected optical axis positions (X/L = 0.25, 0.50, and 0.75) for two selected time instants (t = 100 and 200 ps). The time needed for the laser impulse passing through the medium is $t = L/c$ = 46.7 ps. Thus the deposited energy shown here is the radiation due to multiply scattering events. It is seen that each profile is nearly symmetric against the y and z axes. There is a gradual decrease in divergence of radiative heat flux from the square center to the corner for all the planes because the original incident laser passed through the square centers. At the plane of $X/L = 0.50$, the divergence of radiative heat flux is greatly concentrated at the central inhomogeneous zone because a relatively strong absorbing inhomogeneous zone is embedded. The magnitude of the central plane energy deposition is much larger than those at the planes of $X/L = 0.25$ and 0.75 even though the plane of $X/L = 0.25$ is closer to the incident laser spot. This quantitative analysis is useful for the application of ultrafast lasers in photodynamic therapy. Such a concentration of energy deposition at the cubic center does not exist for the homogeneous medium model. An irradiance field can be easily derived from the radiation deposition field, and vice versa.

The shapes of the logarithmically varied temporal divergence of radiative heat flux at different optical axis positions are compared in Fig. 11. Comparison is also conducted between the homogeneous and inhomogeneous models. It is seen that the peak magnitude of divergence of radiative heat flux decreases with the increase of the X position for the homogeneous model. With the presence of an inhomogeneity, however, the peak value at the inhomogeneous zone position ($X/L = 0.5$) has an abrupt increase even

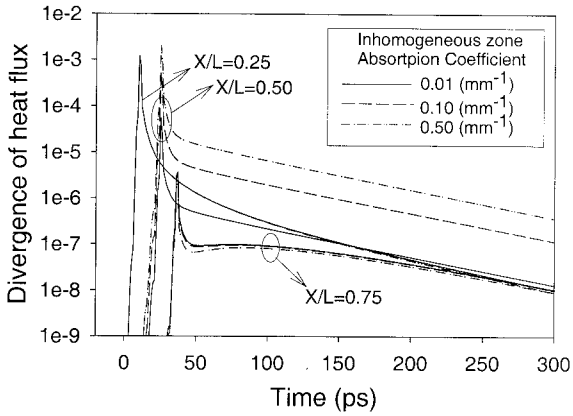

Fig. 11. Comparison of temporal profiles of divergence of radiative heat flux at different optical axis locations with different absorption coefficients in the inhomogeneity.

though the irradiance is much lower at $X/L = 0.5$ than at $X/L = 0.25$. At $X/L = 0.5$, the difference in divergence of radiative heat flux between inhomogeneous and homogeneous models is large. At X/L = 0.25, however, such a difference is nearly invisible. At $X/L = 0.75$, the radiation energy deposition declines substantially. After passing the peak value, the radiation deposition decays in a nearly exponential form.

4. Conclusions

The discrete-ordinates method (DOM) has been developed to study ultrafast-laser-radiation propagation and light energy transfer in 3D scattering, absorbing, and emitting media subject to specularly and/or diffusely reflecting boundary conditions. The time-dependent radiation field such as the radiation energy deposition rate and irradiance inside the tissue, and reflectance and transmittance at the boundary, can be predicted accurately and simultaneously by the present method. Three-dimensional simulations are conducted for both the homogeneous model and the inhomogeneous model with a small inhomogeneity embedded in the center of the homogeneous tissue. It is found that the peak position and temporal shape of the reflectance and/or transmittance are greatly influenced by the presence of the inhomogeneous zone. The time-dependent AVLS of the reflectance and transmittance at the boundaries converges to a constant value after a period of impulse irradiation for a finite-thickness tissue. This constant value varies when there is an embedded inhomogeneity. But the value is irrelevant to the detector position. Further, it is almost linearly proportional to the absorption coefficient of the small inhomogeneity. With the presence of an absorbing inhomogeneous zone such as malignant tumors embedded in healthy tissue, the change of AVLS may be detected, and this concept may be used for the design of a new technique for detecting small tumors or abnormalities.

Simulations in 2D heterogeneous configurations

are made of four different tissue layers. The orientation of heterogeneity of the tissue significantly affects the radiation field and radiation intensity at the boundary. The Fresnel specularly reflecting boundary effect is even stronger than the effect of the internal structure difference at some detector positions. The reflectance and transmittance under the specularly reflecting boundary condition are greater than those under the diffusely reflecting boundary condition. The boundary effect is particularly obvious in the less scattering and absorbing CSF layer. Adequate incorporation of radiation-transfer boundary conditions is extremely important for accurate prediction of photon transport and light imaging wherever tissue–air interfaces are present.

Z. Guo acknowledges support from the Charles and Johanna Busch Memorial Fund Award managed at Rutgers and the Industrial University Research Award from the New Jersey Space Grant Consortium.

References

1. S. R. Arridge and J. C. Hebden, "Optical imaging in medicine. II. modeling and reconstruction," Phys. Med. Biol. **42,** 841–853 (1997).
2. R. R. Alfano, S. G. Demos, and S. K. Gayen, "Advances in optical imaging of biomedical media," Ann. N.Y. Acad. Sci. **820,** 248–270 (1997).
3. M. S. Patterson, B. Chance, and B. C. Wilson, "Time resolved reflectance and transmittance for the noninvasive measurement of tissue optical properties," Appl. Opt. **28,** 2331–2336 (1989).
4. S. L. Jacques, "Time resolved propagation of ultrashort laser pulses within turbid tissues," Appl. Opt. **28,** 2223–2229 (1989).
5. D. M. Rector, R. F. Rogers, and J. S. George, "A focusing image probe for assessing neural activity *in vivo*," J. Neurosci. Methods **91,** 135–145 (1999).
6. A. D. Klose, U. Netz, J. Beuthan, and A. H. Hielsher, "Optical tomography using the time-independent equation of radiative transfer. 1. Forward model," J. Quant. Spectrosc. Radiat. Transfer **72,** 691–713 (2002).
7. F. H. Loesel, F. P. Fisher, H. Suhan, and J. F. Bille, "Nonthermal ablation of neural tissue with femtosecond laser pulses," Appl. Phys. B **66,** 121–128 (1998).
8. K. M. McNally, B. S. Sorg, A. J. Welch, J. M. Dawes, and E. R. Owen, "Photothermal effects of laser tissue soldering," Phys. Med. Biol. **44,** 983–1002 (1999).
9. S. Grapengiesser, F. Gudmundsson, O. Larko, M. Ericson, A. Rosen, and A. M. Wennberg, "Pain caused by photodynamic therapy of skin cancer," Clin. Exp. Dermatol. **27,** 493–497 (2002).
10. A. Obana and Y. Gohto, "Scanning laser system for photodynamic therapy of choroidal neovascularization," Lasers Surg. Med. **30,** 370–375 (2002).
11. E. J. Seibel and Q. Y. J. Smithwick, "Unique features of optical scanning, single fiber endoscopy," Lasers Surg. Med. **30,** 177–183 (2002).
12. S. Kim, E. A. A. Nollen, K. Kitagawa, V. P. Bindokas, and R. I. Morimoto, "Polyglutamine protein aggregates are dynamic," Nat. Cell Biol. **10,** 826–831 (2002).
13. S. T. Flock, M. S. Patterson, B. C. Wilson, and D. R. Wyman, "Monte-Carlo modeling of light propagation in highly scattering tissues. I. Prediction and comparison with diffusion theory," IEEE Trans. Biomed. Eng. **36,** 1162–1168 (1989).
14. D. A. Boas, J. P. Culver, J. J. Stott, and A. K. Dunn, "Three dimensional Monte Carlo code for photon migration through complex heterogeneous media including the adult human head," Opt. Express **10,** 159–170 (2002), http://www.opticsexpress.org.
15. Z. Guo, S. Kumar, and K.-C. San, "Multi-dimensional Monte Carlo simulation of short pulse laser radiation transport in scattering media," J. Thermophys. Heat Transfer **14,** 504–511 (2000).
16. A. Ishimaru, *Wave Propagation and Scattering in Random Media* (Academic, New York, 1987).
17. K. M. Yoo, F. Liu, and R. R. Alfano, "When does the diffusion approximation fail to describe photon transport in random media," Phys. Rev. Lett. **64,** 2647–2650 (1990).
18. M. F. Modest, *Radiative Heat Transfer* (McGraw-Hill, New York, 1993), Chap. 15.
19. W. A. Fiveland, "The selection of discrete ordinate quadrature sets for anisotropic scattering," American Society of Mechanical Engineers, Heat Transfer Division **72,** 89–96 (1991).
20. K. D. Lathrop, "Spatial differencing of the transport equation: positive vs accuracy," J. Comput. Phys. **4,** 475–498 (1968).
21. K. D. Lathrop and F. W. Brinkley, "TWOTRAN-II code," Los Alamos Scientific Laboratory Rep. #LA-4848-MS (Los Alamos Scientific Laboratory, Los Alamos, N. Mex., 1973).
22. S. Kumar and K. Mitra, "Microscale aspects of thermal radiation transport and laser applications," Adv. Heat Transfer **33,** 187–294 (1998).
23. K. Mitra and S. Kumar, "Development and comparison of models for light-pulse transport through scattering–absorbing media," Appl. Opt. **38,** 188–196 (1999).
24. Z. Guo and S. Kumar, "Discrete-ordinates solution of short-pulsed laser transport in two-dimensional turbid media," Appl. Opt. **40,** 3156–3163 (2001).
25. Z. Guo and S. Kumar, "Three-dimensional discrete ordinates method in transient radiative transfer," J. Thermophys. Heat Transfer **16,** 289–296 (2002).
26. J. C. Chai, H. S. Lee, and S. V. Patankar, "Ray effect and false scattering in the discrete ordinates method," Numer. Heat Transfer Part B **24,** 373–389 (1993).
27. A. H. Hielscher, R. E. Alcouffe, and R. L. Barbour, "Comparison of finite-difference transport and diffusion calculations for photon migration in homogeneous and heterogeneous tissues," Phys. Med. Biol. **43,** 1285–1302 (1998).
28. Z. Guo and S. Kumar, "Equivalent isotropic scattering formulation for transient short-pulse radiative transfer in anisotropic scattering planar media," Appl. Opt. **39,** 4411–4417 (2000).
29. S. K. Wan, Z. Guo, S. Kumar, J. Aber, and B. A. Garetz, "Detecting inhomogeneities in a turbid medium," presented at Eurotherm 73 on Computational Thermal Radiation in Participating Media, Mons, Belgium, 15–17 April 2003.